actuators

MDPI

Article

Investigation and Optimization of Energy Consumption for Hybrid Hydraulic Excavator with an Innovative Powertrain

Van Hien Nguyen [1], Tri Cuong Do [1,2] and Kyoung Kwan Ahn [3,*]

[1] Graduate School of Mechanical and Automotive Engineering, University of Ulsan, Ulsan 44610, Republic of Korea; van-hien.nguyen@lqdtu.edu.vn (V.H.N.); cuongdt298@ueh.edu.vn (T.C.D.)
[2] College of Technology and Design, University of Economics Ho Chi Minh City, Ho Chi Minh City 700000, Vietnam
[3] School of Mechanical Engineering, University of Ulsan, Ulsan 44610, Republic of Korea
* Correspondence: kkahn@ulsan.ac.kr; Tel.: +82-52-259-2282

Abstract: This paper presents an innovative powertrain design and an energy regeneration system for hybrid hydraulic excavators to reduce energy consumption and emissions. The proposed system is designed to maximize engine efficiency and make full use of the energy gained from boom and arm retraction. The powertrain features an innovative design that incorporates a continuously variable transmission (CVT), which drives the main pump. It enables precise control of both the engine's speed and torque, ensuring that the engine operates within the high-efficiency range. The energy regeneration system is applied to regenerate the potential energy of the boom and arm, which can be used to either charge the battery or directly supply power to the main pump. Moreover, an energy management strategy based on an equivalent consumption minimization strategy is used to distribute the power while offering maximum engine efficiency. When compared with the existing hybrid system and conventional system, the simulation results indicated that the proposed approach achieves energy-saving efficiencies of 16.9% and 77.1%, respectively, at high velocities and 22.25% and 53.5%, respectively, at medium velocities. This research signifies a promising advancement for sustainable and efficient hydraulic excavator operations.

Keywords: fuel consumption; energy management; energy recuperation; hybrid hydraulic excavators; equivalent factor

MSC: 93C35; 93C40

Citation: Nguyen, V.H.; Do, T.C.; Ahn, K.K. Investigation and Optimization of Energy Consumption for Hybrid Hydraulic Excavator with an Innovative Powertrain. *Actuators* **2023**, *12*, 382. https://doi.org/10.3390/act12100382

Academic Editor: Tatiana Minav

Received: 2 September 2023
Revised: 27 September 2023
Accepted: 5 October 2023
Published: 10 October 2023

1. Introduction

The increasing global energy crisis and environmental pollution, necessitate innovative solutions, particularly in industries such as construction and agriculture where heavy machinery contributes significantly to these issues [1–3]. Research into energy-saving technologies and emission reductions for hydraulic excavators is particularly critical [4–6].

Hybrid technology has emerged as a promising solution to reduce energy consumption in hydraulic excavators ((HEs)) [7,8]. HEs, mainly divided into hydraulic and electric hybrids, have been developed and commercialized, offering potential energy savings [9,10]. Researchers have effectively demonstrated the potential of electric energy regeneration systems (EERSs) within the boom system of hybrid hydraulic excavators (HHEs) in previous studies [11–13]. The EERSs offer efficient energy conservation capabilities and are compatible with electric HHEs. In this application, the energy generated during operation is stored in a battery and subsequently utilized by an electric motor for a future use [3,14,15].

The implementation of energy regeneration systems, such as EERSs and hydraulic energy regeneration systems (HERSs), has been key to HHEs [16,17]. An electric generator in an EERS can be utilized to capture and store the energy that has been regenerated. The

storage options include devices such as a battery or a supercapacitor [18,19]. When considering HERSs, it is notable that the use of hydraulic valves enables the storage of regenerated energy in a hydraulic accumulator [7,20,21]. These systems can capture and store energy that can be used to run actuators directly or assist the internal combustion engine (ICE), thus reducing energy consumption. However, the focus on energy regeneration efficiency often overlooks the need to examine energy reuse in the drive mode, which influences the overall system's energy-saving efficiency [14,22]. An electric hybrid hydraulic excavator was proposed, which considered the ICE and hydraulic pump (HPu) efficiency to enhance energy saving [14]. This system saved 36.69–45.16% of energy compared to conventional systems. Yu et al. also proposed a powertrain, the electrical hydraulic continually variable powertrain (EHCVP), which used an ICE and an electric motor/generator (EMG) to power the boom system. This system could adjust the torque and speed of the ICE for optimal efficiency and regenerate potential hydraulic energy from the boom cylinder, converting it into electrical energy. The generated energy was then stored in a battery for reuse in subsequent cycles. A schematic diagram of an EHCVP system can be seen in Figure 1a. A variable HPu is used to ensure that the speed and torque of the ICE are independent of the pump's speed and load, respectively. The HPu is driven directly by the ICE to supply energy to the hydraulic system without a gearbox. The EHCVP system employs an EMG capable of operating as both a motor and a generator, enabling the generation of mechanical or electric energy. By employing the EHCVP system, it became possible to adjust the operating speed of the ICE to operate optimally. Additionally, the system incorporated a pump capable of altering its displacement, which allowed for precise control over the torque produced by the ICE. This allows for the ICE to operate in its high-efficiency range. However, one should bear in mind that the range of torque control in the ICE at high speeds is constrained by the maximum displacement of the HPu. Under the conditions of an extremely large load and middle velocity, the EHCVP could not control the ICE to work with higher efficiency, highlighting the need for further research. Moreover, despite extensive research on energy regeneration systems, further exploration remains necessary to enhance the efficiency of energy utilization in HHEs, particularly with respect to energy reuse during the drive mode [3].

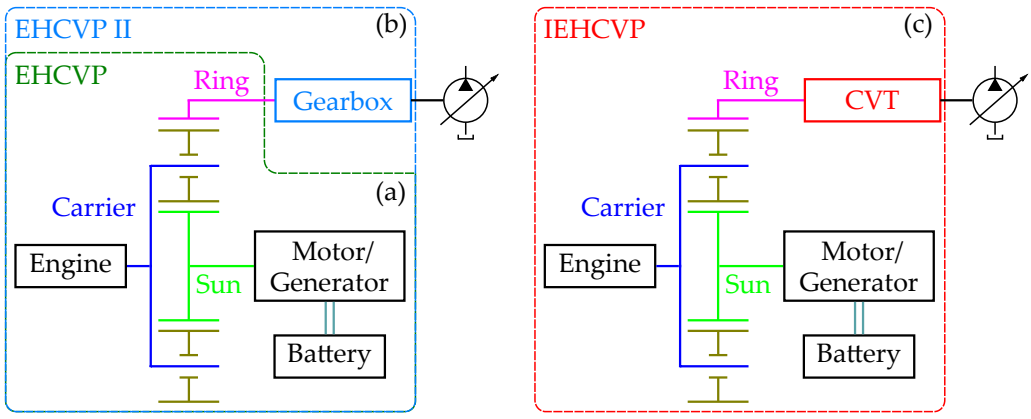

Figure 1. Comparison of the powertrain of the EHCVP, EHCVP II, and proposal structures.

To overcome the drawbacks of the EHCVP system, Yu et al. proposed an improved version of the EHCVP, called the EHCVP II system [23]. This system incorporated a two-speed gearbox, situated between the planetary gearbox and the HPu, which primarily governed the control of the ICE torque, as illustrated in Figure 1b. Additionally, the speed of the ICE was controlled by the EMG. The EHCVP II system was demonstrated to effectively decrease energy usage when operating at high speeds. In comparison to both the existing EHCVP system and a conventional system, it achieved energy savings of 11% and 54%, respectively, under high-speed conditions. Thus, the EHCVP II system offered an efficient solution for reducing fuel consumption in hydraulic excavators. However, its ability to

reduce energy consumption was not prominent at medium and low speeds. Furthermore, the EHCVP II only considered the energy regeneration mode with a standalone boom system. In the case of the arm and bucket working, the energy regeneration mode of the boom cylinder could not operate. The ICE and EMG can both independently operate the HPu or work in unison with each other. While implementing the EHCVP II, the two-speed gearbox's capability to adapt to different speeds may be limited. Consequently, its effectiveness in reducing energy consumption might not be prominent, particularly at medium and low speeds. Additionally, using 1:1 gear ratios for energy regeneration may lead to decreased generator efficiency. This makes it extremely challenging to implement these systems on real excavators.

At higher velocities, the efficiency of the engine decreases as a result of its increased speed. One possible solution to address this issue is to introduce an HPu with a larger capacity into the system to enhance the ICE's efficiency at high speeds. However, it should be noted that the hydraulic pump primarily operates at low and medium displacements, leading to lower efficiency under other conditions. As a result, the existing design limitations of these systems hinder the potential improvement of energy-saving efficiency, particularly when operating at high velocities. Consequently, it may not be possible to enhance the fuel consumption of the entire system across different velocities in real-world engineering applications.

To enhance the energy-saving efficiency of hybrid systems, numerous energy management strategies have been suggested, as pointed out in source [24]. The role of an energy management strategy (EMS) is of paramount importance in bolstering the energy-saving efficiency in such hybrid systems. One prominent example of an energy management strategy is the equivalent consumption minimization strategy (ECMS) utilized to regulate hybrid systems, which uses an equivalent factor (EF) to convert battery electrical energy into fuel consumption [25]. However, the traditional ECMS approach bears constraints owing to the use of a static EF that has been predetermined under certain specific conditions through offline optimization. The Adaptive ECMS (A-ECMS), which dynamically updates the EF, involves conducting several experiments to determine values such as the starting EF and the coefficient of proportionality [26]. A method for updating the EF, which relies on velocity prediction, has been suggested [27], providing temporary driving information for the real-time EF and achieving a stable state-of-charge (SOC) trajectory. Tian X. et al. [28], introduced an approach wherein the A-ECMS was dependent on the driving style, updating the EF accordingly. This strategy resulted in better fuel economy and a more stable SOC. Energy regeneration and energy reuse of drive mode are important for deciding the energy-saving efficiency. The existing research has not optimized energy working points, considering pump efficiency, in the structure design and EMS for an engine-driven excavator [22,29,30]. Developing a new HE with high efficiency and stability requires a new powertrain and EMS [31,32]. Several methods have been proposed for optimal power distribution in a hybrid powertrain [33,34], but they require prior knowledge of the drive cycle and offline optimization.

ECMS has been implemented in parallel hybrid forklifts and parallel powertrain HEs to minimize fuel consumption and regulate the SOC of the supercapacitor within the optimal range. This is achieved by adjusting the engine speed based on the load condition [35]. Extremum seeking (ES) is a model-free, real-time EMS also suitable for complex systems, such as HEs [36]. Global optimal solutions cannot be directly applied in a real-time EMS; however, they serve as valuable reference points for comparing and evaluating other strategies. In a study conducted by Anders et al. [37], an ECMS was utilized in a parallel powertrain HE, taking into account the power consumption of the ICE and the electric motor's internal and kinetic power, all incorporated within a Hamiltonian function.

To address the previously mentioned challenges and to effectively minimize fuel consumption in HHEs, this research proposes an innovative solution aimed at reducing fuel consumption in HHEs. The main contributions of the article are presented as follows:

- This solution stands out by prioritizing energy regeneration and optimization of energy reuse for both boom and arm operations. By considering the energy regeneration mode for not only the standalone boom system but also the arm working scenarios, the solution ensures maximum efficiency in energy utilization.
- The powertrain design employs a CVT, which allows for precise control over the ICE's speed and torque. This ensures that the ICE always operates within its highest efficiency range, thereby minimizing fuel usage.
- By optimizing the ICE working points, it utilizes an ECMS integrated with a CVT system to maximize the energy-saving efficiency and implement energy regeneration. Consequently, this approach can significantly reduce the energy expenditure of such HHEs. The IEHCVP system demonstrates an improved energy consumption reduction even at medium and low speeds.

When compared with both the EHCVP II setup and traditional excavator configurations, the proposed system achieves remarkable energy savings of 16.9% and 77.1%, respectively, at high velocities, and 22.25% and 53.5%, respectively, at medium velocities.

This paper is structured as follows. Firstly, Section 2 provides a comprehensive discussion of the previous systems and the proposed innovative powertrain enhancement for the EHCVP. The energy management strategy is presented in Section 3. In Section 4, simulations and discussions are conducted to validate the system's performance, and a comparison of the energy efficiencies is made between the systems. Finally, our conclusions are presented in Section 5.

2. Proposal System Configuration

To optimize energy-saving efficiency, particularly in scenarios involving high and medium velocities as well as heavy loads, this paper introduces an innovative EHCVP structure for the boom and arm systems. The proposed structure, depicted in Figure 2, enables energy regeneration from boom retraction and facilitates its reuse for the arm-up mode, and vice versa, simultaneously. The innovative EHCVP has the ability to harness energy during boom descent. It can supply mechanical power to drive the pump and also generate electrical power to charge the battery. The hydraulic motor (HMo) is installed in the return line of the boom and arm cylinders to regenerate the potential energy of the boom and arm systems, respectively. Simultaneously, a gearbox is installed in the return line of the boom and arm cylinder to reverse the torque of the HMo, thereby facilitating energy reuse for the battery and HPu. Not only does it have the features previously mentioned, but the IEHCVP also includes a CVT, which is located in the position connecting the planetary gearbox to the HPu. The CVT, together with the HPu, primarily regulates the ICE torque, enabling more flexible control of the ICE torque's working range compared to the current EHCVP II. Furthermore, the speed of the ICE is governed by the EMG. The proposed innovative powertrain enhancement for EHCVP in this paper is named the IEHCVP. With the IEHCVP, the CVT can adjust the ICE's speed and torque over a wide range of gear ratios at high velocities. This allows the ICE to operate more efficiently at high speeds. In the mid-range and low-speed conditions, the proposed IEHCVP can maintain a high level of efficiency compared to the current EHCVP II. Overall, in real-world engineering applications, the IEHCVP demonstrates enhanced fuel efficiency across a range of velocities, adapting to varying operating conditions.

In the IEHCVP configuration, various elements, such as the ICE, the EMG, and the CVT, are specifically associated with the carrier, the sun, and the ring, in that order. The rotational velocities of these gears are dictated by Equation (1) [23].

$$\omega_{rg} \times d_{rg} = \omega_{ca} \times \left(d_{rg} + d_{sg}\right) - \omega_{sg} \times d_{sg} \quad (1)$$

where we take into consideration the diameter and speed, which are represented as d_{sg} and ω_{sg} for the sun gear, and, similarly, d_{rg} and ω_{rg} for the ring gear. The speed at which the carrier moves is denoted as ω_{ca}.

The ratio of the CVT follows Equation (2).

$$\omega_{\mathrm{rg}} = i_{\mathrm{cvt}}\omega_{\mathrm{Hpu}} \tag{2}$$

where ω_{Hpu} stands for the HPu's speed and i_{cvt} represents the ratio of the CVT. The joystick signal provides the desired flow rate, which is in line with Equation (3).

$$\omega_{\mathrm{Hpu}} = \frac{q_{\mathrm{c}}}{D_{\mathrm{Hpu}}\eta_{\mathrm{Hpuv}}} \tag{3}$$

where η_{Hpuv} and q_{c} denote the HPu's efficiency in terms of volume and its rate of flow, respectively. Using Equations (2) and (3), the selection of the HPu's displacement and the CVT's ratio can be determined from the required rate of flow. This results in an infinite number of possible combinations for the ICE speed and the speed of the EMG, as guided by Equation (1). The control strategy then defines the final command for the speed of both the ICE and the EMG.

Each gear's torque is dictated by Equation (4) [38].

$$T_{\mathrm{rg}} : T_{\mathrm{sg}} : T_{\mathrm{ca}} = d_{\mathrm{rg}} : d_{\mathrm{sg}} : \left(d_{\mathrm{rg}} + d_{\mathrm{sg}}\right) \tag{4}$$

where T_{rg}, T_{sg}, and T_{ca} represent the torques corresponding to the elements of the ring, sun gears, and carrier, in that order. The HPu's torque depends on the pressure at the HPu's output side, as demonstrated in Equation (5).

$$T_{\mathrm{rg}} = \frac{T_{\mathrm{Hpu}}}{i_{\mathrm{cvt}}} = \frac{p_{\mathrm{c}}D_{\mathrm{Hpu}}}{2\pi\eta_{\mathrm{Hpum}}i_{\mathrm{cvt}}} \tag{5}$$

where T_{Hpu} symbolizes the torque associated with the HPu, and p_{c} reflects the pressure on the HPu's output side. Further, D_{Hpu} conveys the HPu's displacement, while η_{Hpum} accounts for the HPu's hydro-mechanical efficiency. The torque HPu, denoted by T_{Hpu}, governs the torque of the ring gear.

In the test simulation, a large and small cylinder are utilized to replicate the boom and arm cylinder, respectively, as found in the real system in the laboratory. EMG #1 and #2 are used to simulate the functionalities of the ICE and the combined motor/generator, correspondingly. Meanwhile, the load is fastened to the cylinder's rod. The planetary gear output shaft is regulated by a CVT, which can connect it to either the HPu or the HMo. When the CVT is connected to the HPu, it operates in a mode called 'boom-up' or 'arm-up'. During this phase, the valves VB and VA are positioned on the left. The function of the IEHCVP is to propel the HPu, enabling the elevation of the load. Conversely, when the CVT engages with the HMo, the system switches into either 'boom-lowering' mode, 'arm-lowering' mode, or both modes. In this state, the energy recuperation valves, namely VGB and VGA, become operational. This facilitates the transfer of fluid from the cylinder to the HMo. The latter is linked to both the innovative powertrain and the HPu. The purpose of VGB and VGA is to reduce the flow rate through the HMo, especially under high velocity and heavy load conditions. This ensures system safety and minimizes the power required to drive the generator. EMG #2 acts as a generator in this scenario to stabilize the torque from the HMo while also recapturing energy. The HMo propels either EMG #2 through the CVT and planetary gear or the arm cylinder through BrakeP and the HPu. Each gear shaft within the planetary system is equipped with devices to measure speed and torque and a pressure monitoring device positioned within the discharge port of the rod chamber in the boom and arm cylinders.

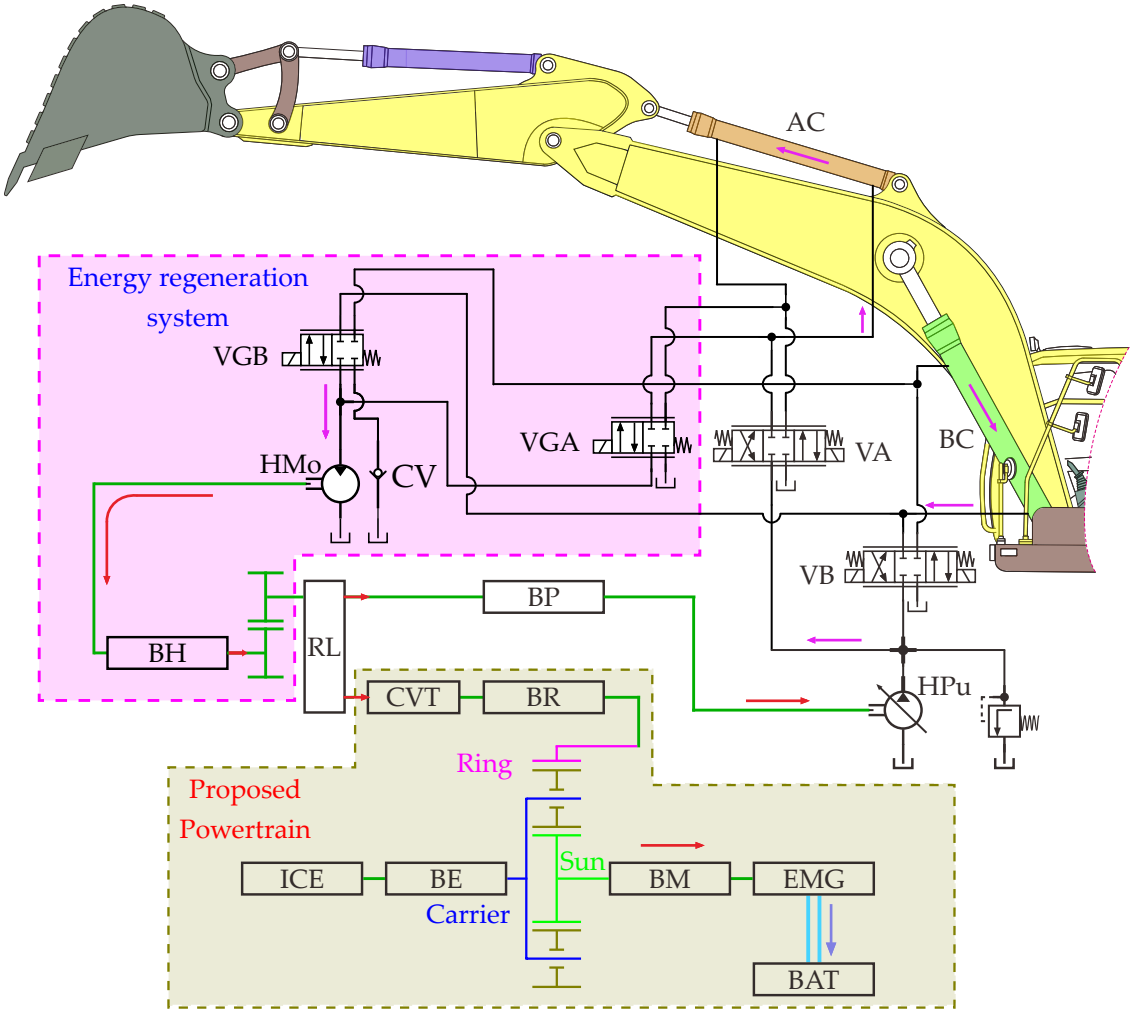

Figure 2. Structure of the IEHCVP.

3. Energy Management System

3.1. Discussion and Control Modes of IEHCVP System

When operating in boom and arm-up mode, the velocity of the cylinders is directly proportional to the joystick signal, as expressed in Equation (6).

$$v_r = \alpha v_{max} \tag{6}$$

where α represents the joystick signal, while v_r and v_{max} correspond to the cylinders' desired velocity and their maximum velocity, in that order. The α value spans from 0 to a full 100%. Furthermore, the necessary rate of flow q_c can be determined using Equation (7).

$$q_c = v_r A_{cr} \tag{7}$$

where the area of the rod chamber is denoted by A_{cr}. The speed of the HPu can be calculated using Equation (3). In order to achieve the needed flow rate while enhancing the system's energy efficiency, it is necessary to control the ICE speed, EMG speed, CVT, and displacement of the HPu. Therefore, an energy management strategy must be implemented for the IEHCVP system. Furthermore, the pressure p_c can be determined using Equation (8).

$$p_c = \frac{F}{A_{cr}} \tag{8}$$

where F represents the force acting on the cylinder.

This article discusses the control mode of the IEHCVP system and its components, as illustrated in Figure 3. The lifting process can be executed by utilizing the energy supplied by the ICE, the electric motor, or the energy of the arm when moving downwards. It can also be accomplished by a combination of two of the three aforementioned sources. Similarly, for the arm, energy can be derived from the ICE, electric motor, or boom. Modes b1 and b2 exclusively utilize either the ICE or the electric motor to power the boom-up mode, respectively. In b3, both the ICE and the electric motor are combined to provide the necessary power. In b4, the ICE provides the necessary power for the boom and the battery. As for b5 and b6, the arm, in combination with either the ICE or the electric motor, respectively, exclusively powers the mode. Lastly, b7 is a mode where only the arm provides the required power. Similarly, modes a1, a2, and a3 exclusively utilize the ICE, the electric motor, and the boom to power the arm-up mode, respectively. Operation Mode, please refer to the Table 1 below.

Table 1. Operation mode.

Operation Mode	Functional	Symbols
Engine mode	Boom cylinder supplied by only engine Brake BE, BR, BP operate	b1
Motor mode	Boom cylinder supplied by only electric motor Brake BM, BR, BP operate	b2
Hybrid mode #1	Boom cylinder supplied by both engine and electric motor Brake BE, BM, BR, BP operate	b3
Hybrid mode #2	The engine supplies power to the boom cylinder and the battery Brake BE, BM, BR, BP operate	b4
Arm_reuse_Motor mode	Boom cylinder is powered by both the electric motor and the arm when the arm is lowering Brake BM, BR, BH, BP operate	b5
Arm_reuse_Engine mode	Boom cylinder is powered by both the engine and the arm when the arm is lowering Brake BE, BR, BH, BP operate	b6
Arm mode	Boom cylinder is powered solely by the arm when the arm is lowering Brake BH, BP operate	b7
Boom_reuse_Generator mode	Boom cylinder supplies power to the arm when the arm is raised and also to the battery Brake BM, BR, BH, BP operate	b8
Generator mode	Energy from the lowering of the boom is supplied to the battery Brake BM, BR, BH operate	b9
Engine mode	Arm cylinder supplied by only engine Brake BE, BR, BP operate	a1
Motor mode	Arm cylinder supplied by only motor Brake BM, BR, BP operate	a2
Boom mode	Arm cylinder supplied by only boom when the boom is lowering Brake BR, BH, BP operate	a3
Arm mode	Boom cylinder supplied by only arm when the arm is lowering Brake BH, BP operate	a4
Generator mode	Energy from the lowering of the arm is supplied to the battery Brake BM, BR, BH operate	a5

During the lowering process, the recovered energy can be used to drive the generator and lift the arm, or it can only be used to drive the generator separately. Similarly, for the arm, energy can be used to drive the generator or participate in the lifting process. The recovered energy in mode b8 can be utilized to drive the generator and lift the arm. In mode b9, the recovered energy is solely employed to drive the generator. Similarly, in modes a4 and a5, the recovered energy can be used to drive the generator and lift the boom, respectively.

Corresponding to each of the mentioned modes, the brakes BE, BM, BR, BH, and BP are controlled to turn on or off accordingly, as illustrated in Figure 3.

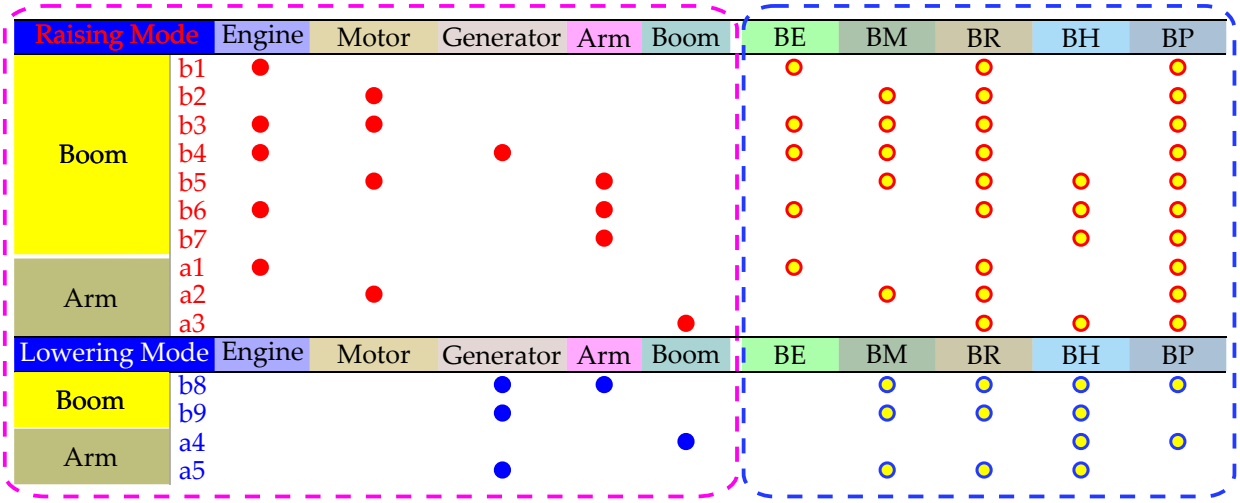

Figure 3. Mode control is used for raising and lowering the boom and arm.

3.2. Strategy for Energy Management

As previously discussed, the EMS significantly influences the energy efficiency of the IEHCVP. An ECMS approach has been employed with the aim of enhancing this efficiency. This ECMS was utilized in the context of a hybrid excavator to ascertain the situation that resulted in the least amount of fuel consumption. Given the unique properties of the IEHCVP, a novel ECMS has been suggested as the strategic approach to energy management. The cost function for the proposed ECMS is detailed in Equation (9) [28].

$$\dot{m}_{\text{total}} = \dot{m}_{\text{e}} + s(t) \times \dot{m}_{\text{m/g}} \tag{9}$$

where $\dot{m}_{\text{total}}$ is the comprehensive equivalent of fuel consumption and $\dot{m}_{\text{e}}$ and $\dot{m}_{\text{m/g}}$ are the equivalent energy consumptions of the ICE and EMG, respectively. The EF, denoted as $s(t)$, is needed to convert the electricity consumption into equivalent fuel consumption, as shown in Equation (10) [39].

$$s(t) = \begin{cases} s_{\text{dis}} \times \left(1 - \left(\frac{SOC - SOC_{\text{ave}}}{4 \times (SOC_{\max} - SOC_{\min})}\right)^3\right), & \omega_{\text{sg}} T_{\text{sg}} > 0 \\ s_{\text{char}} \times \left(1 - \left(\frac{SOC - SOC_{\text{ave}}}{0.5 \times (SOC_{\max} - SOC_{\min})}\right)^3\right), & \omega_{\text{sg}} T_{\text{sg}} \leq 0 \end{cases} \tag{10}$$

where s_{dis} and s_{char} are the discharge coefficient and charging coefficient, respectively, and can be expressed as Equation (11) [40].

$$\begin{cases} s_{\text{dis}} = \frac{1}{\eta_{\text{e}} \times \eta \times \eta_{\text{chg}}}, & \omega_{\text{sg}} T_{\text{sg}} > 0 \\ s_{\text{char}} = \frac{\eta_{\text{mdis}} \times \eta_{\text{dis}}}{\eta_{\text{e}}}, & \omega_{\text{sg}} T_{\text{sg}} \leq 0 \end{cases} \tag{11}$$

where η_{e} is engine efficiency; η_{mchg} is the efficiency of the motor during power generation; η_{mdis} is the efficiency of the motor during driving; and η_{chg} and η_{dis} are the charge and discharge efficiency of the battery, respectively.

The SOC of a lithium-ion battery is a measure of its remaining capacity compared to its fully charged capacity, which needs to be kept within a defined range to provide the required power. The SOC can be expressed as Equation (12) [41], which includes the initial SOC of the battery SOC_{init}; the Coulomb efficiency of the battery η_{b}, which is assumed to be 1 for battery discharging and 0.98 for battery charging; and the power of the lithium-ion battery $P_{\text{m/g}}$, where positive $P_{\text{m/g}}$ values indicate discharging and negative $P_{\text{m/g}}$ values

indicate charging. Additionally, E_b denotes the nominal energy rating of the battery in Watt-hours (Wh).

$$SOC = SOC_{init} + \int_o^t \frac{P_{m/g}}{3600\eta_b E_b} dt \tag{12}$$

where $P_{m/g}$ can be expressed by Equation (13)

$$P_{m/g} = \frac{\omega_{sg} T_{sg}}{9550} \tag{13}$$

In ECMS, $\dot{m}_e$ and $\dot{m}_{m/g}$ can be expressed by Equations (14) and (15) [42].

$$\dot{m}_e = \int \frac{\omega_{ca} T_{ca}}{9550\eta_e} \tag{14}$$

$$\dot{m}_{m/g} = \begin{cases} \int \frac{\omega_{sg} T_{sg}}{9550 \times \eta_{m/g}\eta_b}, & \omega_{sg} T_{sg} > 0 \\ \int \frac{\omega_{sg} T_{sg} \eta_{m/g}\eta_b}{9550}, & \omega_{sg} T_{sg} \leq 0 \end{cases} \tag{15}$$

where $\eta_e, \eta_{m/g}$, and η_b denote the efficiency of the ICE, EMG, and battery, respectively. $\dot{m}_{m/g}$ represents the equivalent output energy of the battery. Regarding Equation (15), if the EMG operates as a motor, the directions of the speed and torque align ($\omega_{sg} T_{sg} > 0$). Conversely, when $\omega_{sg} T_{sg} \leq 0$, it indicates that the EMG functions as a generator. Utilizing Equations (4) and (5), we can calculate T_{ca} and T_{sg}, which are then shown in Equations (16) and (17).

$$T_{ca} = \frac{(d_{rg} + d_{sg}) p_c D_{HPu}}{2\pi i_{cvt} d_{rg} \eta_{Hpum} \eta_{cvt}} \tag{16}$$

$$T_{sg} = \frac{d_{sg} p_c D_{Hpu}}{2\pi i_{cvt} d_{rg} \eta_{Hpum} \eta_{cvt}} \tag{17}$$

In Equations (16) and (17), the pressure sensor measures the cylinder pressure p_c in the IEHCVP. The ECMS of the IEHCVP differs from that of a regular vehicle due to its unique structure. In order to calculate the proposed ECMS, the efficiency of the hydraulic part and CVT must also be taken into account. The proposed ECMS, as described in Equations (9) and (14)–(17), incorporates the ICE efficiency η_{cvt}, battery efficiency, HPu efficiency, battery SOC, CVT efficiency η_{cvt}, and CVT gear ratio. Therefore, by combining the conventional ECMS with the specific characteristics of the IEHCVP, the proposed ECMS aims to reduce fuel consumption. To illustrate the proposed ECMS calculation, a flow chart outlining the essential EMS components is presented in Figure 4.

The i_{sys} transmission ratio of the entire system can be characterized as follows:

$$i_{sys} = i_{cvt} \times i_{plg} \tag{18}$$

where i_{plg} is the ratio of the planetary gearbox.

In Equation (9), the constraints for the system are defined as follows in Equation (19):

$$\begin{cases} SOC_{min} \leq SOC \leq SOC_{max} \\ T_{camin} \leq T_{ca} \leq T_{camax} \\ \omega_{camin} \leq \omega_{ca} \leq \omega_{camax} \\ T_{sgmin} \leq T_{sg} \leq T_{sgmax} \\ \omega_{sgmin} \leq \omega_{sg} \leq \omega_{sgmax} \end{cases} \tag{19}$$

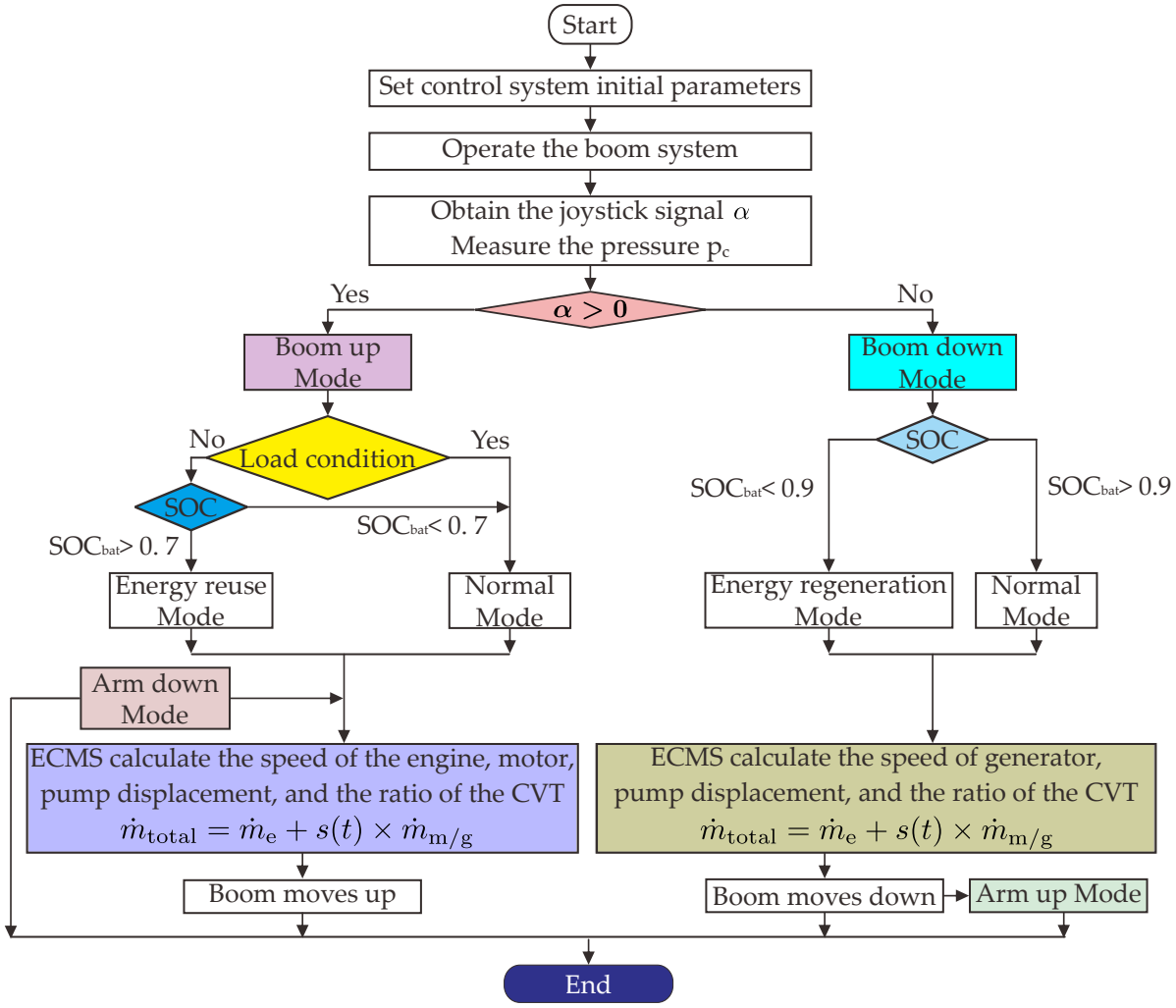

Figure 4. Flow chart of the EMS.

4. Simulation and Discussion

4.1. Investigation of Key Parameters in a Simulation Model

Based on the aforementioned analysis, the ICE speed and torque are decoupled from the pump speed and load, respectively. Moreover, it is possible to achieve energy regeneration, which contributes to a reduction in fuel consumption for HHEs equipped with an IEHCVP.

The ICE's speed range is determined based on the range of the boom cylinder velocity. In the case of the real excavator and the real system in the laboratory, the velocity range of the boom cylinder is between 0.05 and 0.2 m/s. In this simulation, the same velocity range as that of the real system is selected to test the innovative system. The ICE's torque range is chosen based on the load of the simulation. In this case, the load is 30 times smaller than that of a 21-ton hydraulic excavator. To ensure the ICE's optimal working efficiency, the speed and torque ranges should not be excessively large. Therefore, the ranges for the ICE's speed and torque are carefully selected to balance the requirements of velocity, load, and efficiency. In the case of this proposed system using the SAA6D107E-1 engine [43,44], the simulation results are used to scale down the ICE's speed and torque, and the corresponding efficiency map is used to calculate the energy management strategy and to verify the trend in the energy-saving efficiency. The hydraulic system and load sizes in the simulation are the same as those used in the real system. The IEHCVP has the potential to enhance energy efficiency, particularly under conditions of high velocity. The simulation considered a cylinder boom and arm with maximum velocities of 0.2 m/s and loads of 700 kg and 500 kg, respectively. The efficiency maps of the ICE and EMG [45] are

based on those described in the real system. In real engineering, the speed range of an ICE is typically around 800–4000 rpm. However, for the purpose of simulating the real system, the ICE speed range has been limited to 100–500 rpm. The EMG's speed and torque are measured by a speed sensor and a torque sensor to determine the ICE's working points. To verify the energy savings of the IEHCVP, a test simulation model was built using AMESim software version 2022.1, as shown in Figure 5.

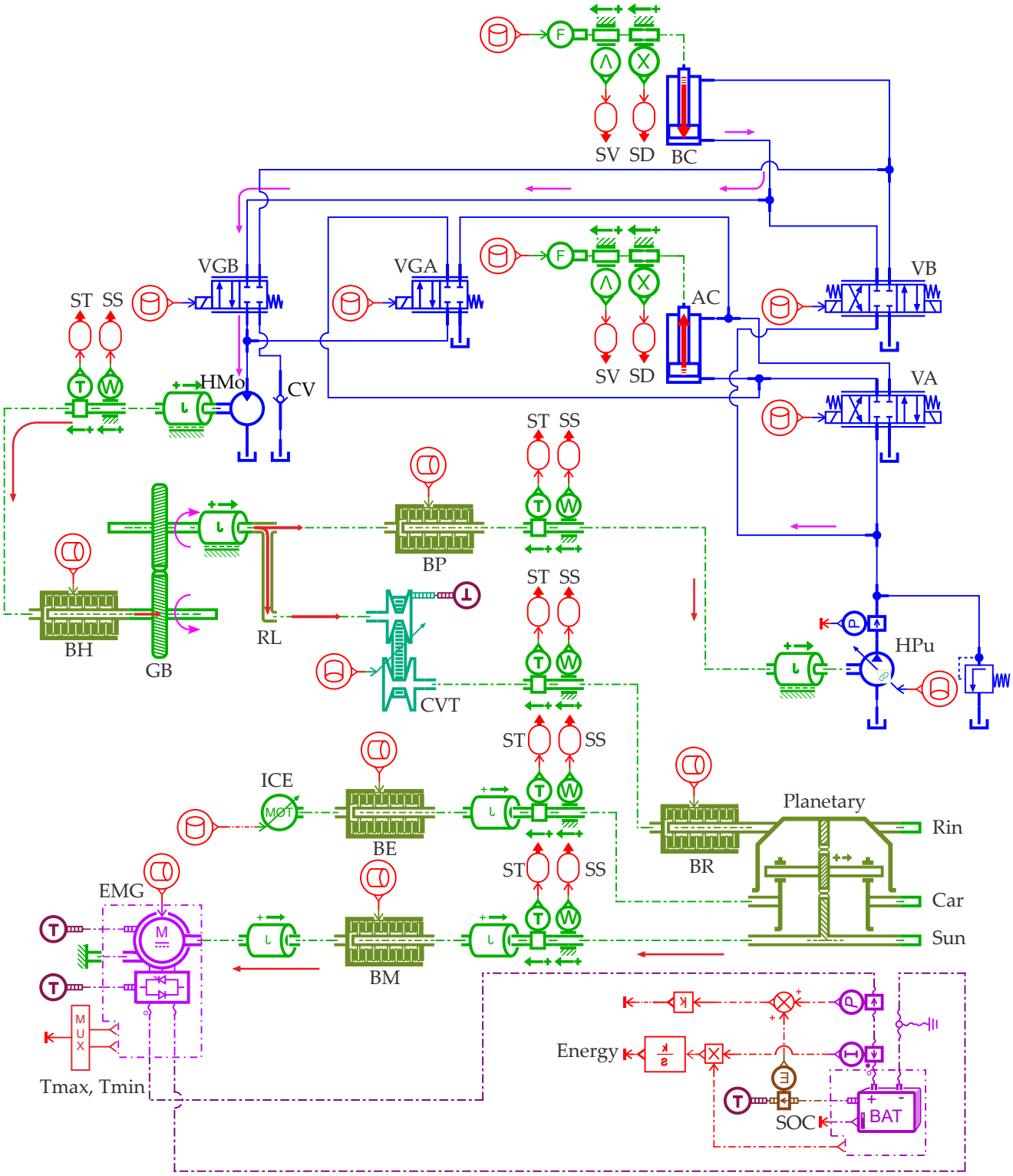

Figure 5. AMESim model of the proposed IEHCVP system.

In the simulation, a variable hydraulic pump is used with a displacement range from 10 to 55 cc/rev. As discussed in Section 3, the proposed energy management strategy takes into account the efficiency of the hydraulic pump. Therefore, the volumetric efficiency and hydro-mechanical efficiency of the hydraulic pump are tested on the simulation and used for calculation in the ECMS. Figure 6 shows one map of the volumetric efficiency and hydro-mechanical efficiency. Function of the key components, please refer to the Table 2 below.

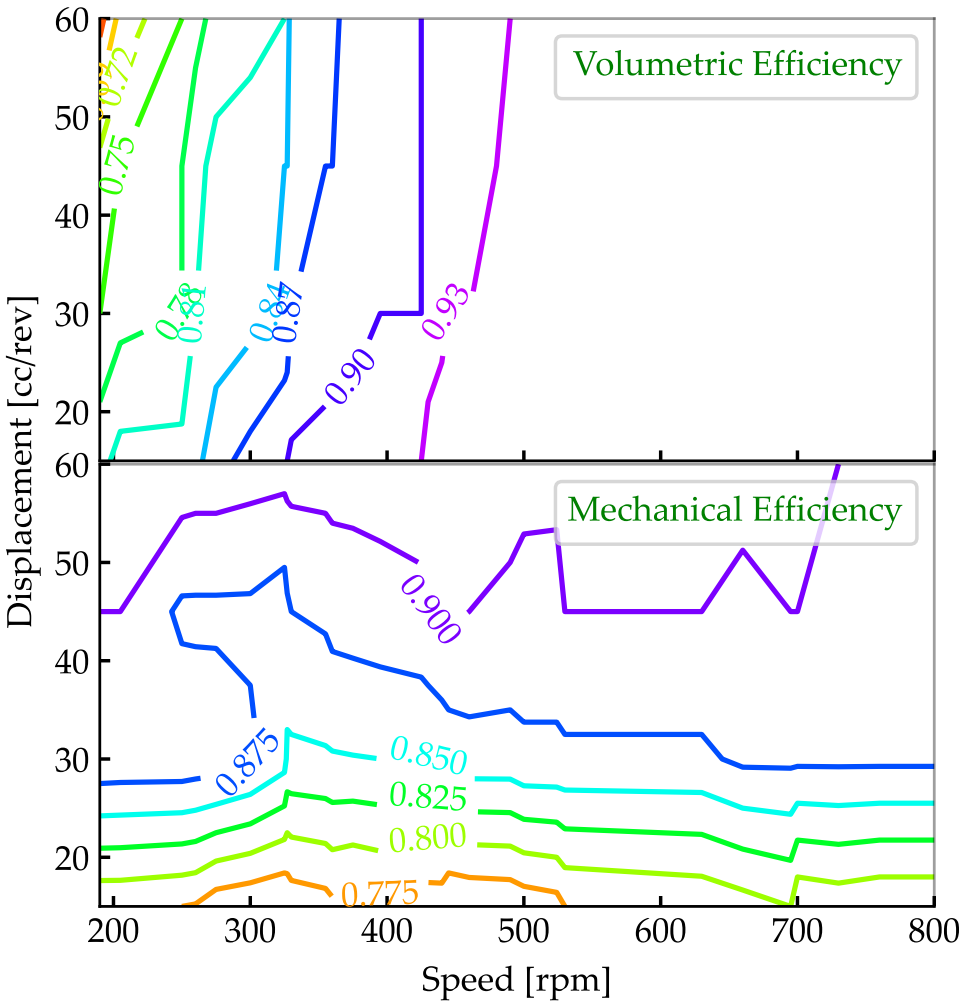

Figure 6. Efficiency of hydraulic pump.

In a hybrid hydraulic excavator, the battery's capacity is a crucial factor to consider. To ensure the battery's longevity and avoid deep discharge and overcharging, the working range of the battery is typically set between 30 and 90% of its total capacity [17,46]. Additionally, the battery must have enough energy to drive the hydraulic excavator through its electric motor. Based on these requirements, a battery with a capacity of 0.02 kWh was chosen for the simulation tests. This battery capacity is sufficient to provide energy for many cycles of operation while remaining within the recommended working range. Table 3 presents the parameters for the main components.

Table 2. Function of the key components.

Component	Functional	Abbreviation
Hydraulic pump	Supply the flow rate to the cylinder	HPu
Hydraulic motor	Convert hydraulic energy into mechanical energy	HMo
Hydraulic boom cylinder	Create linear motion for the boom	BC
Hydraulic arm cylinder	Create linear motion for the arm	AC
Control valve of BC	Change the direction of boom cylinder movement	VBC
Control valve of AC	Change the direction of arm cylinder movement	VAC
Regeneration valve of BC	Transfer flow rate from boom cylinder to hydraulic motor	VGB
Regeneration valve of AC	Transfer flow rate from arm cylinder to hydraulic motor	VGA
Check valve	Installed in pipelines to prevent backflow	CV
Internal combustion engine	Supply main mechanical power to system	ICE
Electric motor/generator	Supply sub-mechanical power to system or Convert mechanical energy into electric energy to battery	EMG
Battery	Store electric energy	BAT
Ring gear	Connect to hydraulic system	Rin
Sun gear	Connect to EMG	Sun
Carrier	Connect to ICE	Car
Continuously variable transmission	Control speed and torque of ICE, EMG	CVT
Rotary link	To connect component of system together also used for torque division	RL
Gearbox	Change the direction of torque from the hydraulic motor to the system	GB
Brake	Connect or disconnect between two shafts	BE, BM, BR, BP, BH

Table 3. Parameters of the key components.

Component	Value	Remark	Unit
Hydraulic pump	30 (IEHCVP)	Displacement	cc/rev
	36 (EHCVP II)	-	-
	55 (Conventional system)	-	-
Hydraulic motor	20	Displacement	cc/rev
Boom cylinder	0.05*0.028*1.0	Piston dia.*Rod dia.*Stroke	m
Arm cylinder	0.03*0.02*0.6 (Arm)	-	-
Control valve of boom/arm cylinder	40	Valve rated current	mA
Regeneration valve of boom/arm cylinder	10	-	-
Check valve	250	Check valve flow rate pressure gradient	L/min/bar
	0.5	Check valve cracking pressure	bar
Motor (Engine)	7.5	Rate power	kW
Motor/Generator	5.5	-	-
Battery	0.02	Capacity	kWh
Planetary geartrain	260 (Ring)	Diameter	mm
	100 (Sun)	-	-
Gearbox	1:1	Ratio	-
Brake	10	Number of clutch contact faces	-
	250	Maximum Coulomb	-

4.2. Simulation Results and Discussion

During the simulation process, the speed and torque sensors are utilized to measure the speed and torque of both the ICE and EMG. The acquired data, along with the control signal from the speed and torque readings obtained from the ICE and EMG sensors, are then fed into an ECMS implemented using Python from Equation (9). The calculation results are then sent back to the control elements in AMESim. This paper presents a novel approach that replaces the conventional Simulink method by leveraging Python co-simulation with AMESim.

The displacement of the boom and arm cylinders is shown in Figure 7a. The velocities for the boom and arm cylinders are 0.2 m/s and 0.12 m/s, respectively, during most cycles.

In the arm-up mode and arm-down mode in the fourth cycle, the velocities are 0.1 m/s and 0.2 m/s, respectively. Specifically, between seconds 1 and 30, the ICE powered both the boom and arm extension, while any energy generated during the retraction process was stored in the battery. From 33 to 38 s, the system operated in boom-up mode, with both the ICE and motor contributing to the energy supply in hybrid mode #1 (ICE + motor). Energy recovered during arm retraction and from the motor was used to lift the boom from seconds 52 to 57, while the energy recovered during boom-down mode regeneration (between 60 and 65 s) was divided into two lines: one line supplied energy to the HPu for extending the arm, while the other charged the battery. From seconds 68 to 73, the energy needed to lift the boom was obtained from energy recovered during arm retraction and from the ICE. The motor provided energy for extending the arm between seconds 82 and 88. From 91 to 94 s, the energy needed for lifting the boom was obtained from the energy recovered during the arm retraction. From seconds 94 to 99, the ICE provided the energy required for lifting the boom. Finally, from seconds 114 to 119, the ICE powered the boom, charging the battery simultaneously, as hybrid mode #2 (ICE + generator). A conventional system without the EHCVP II and IEHCVP was also tested.

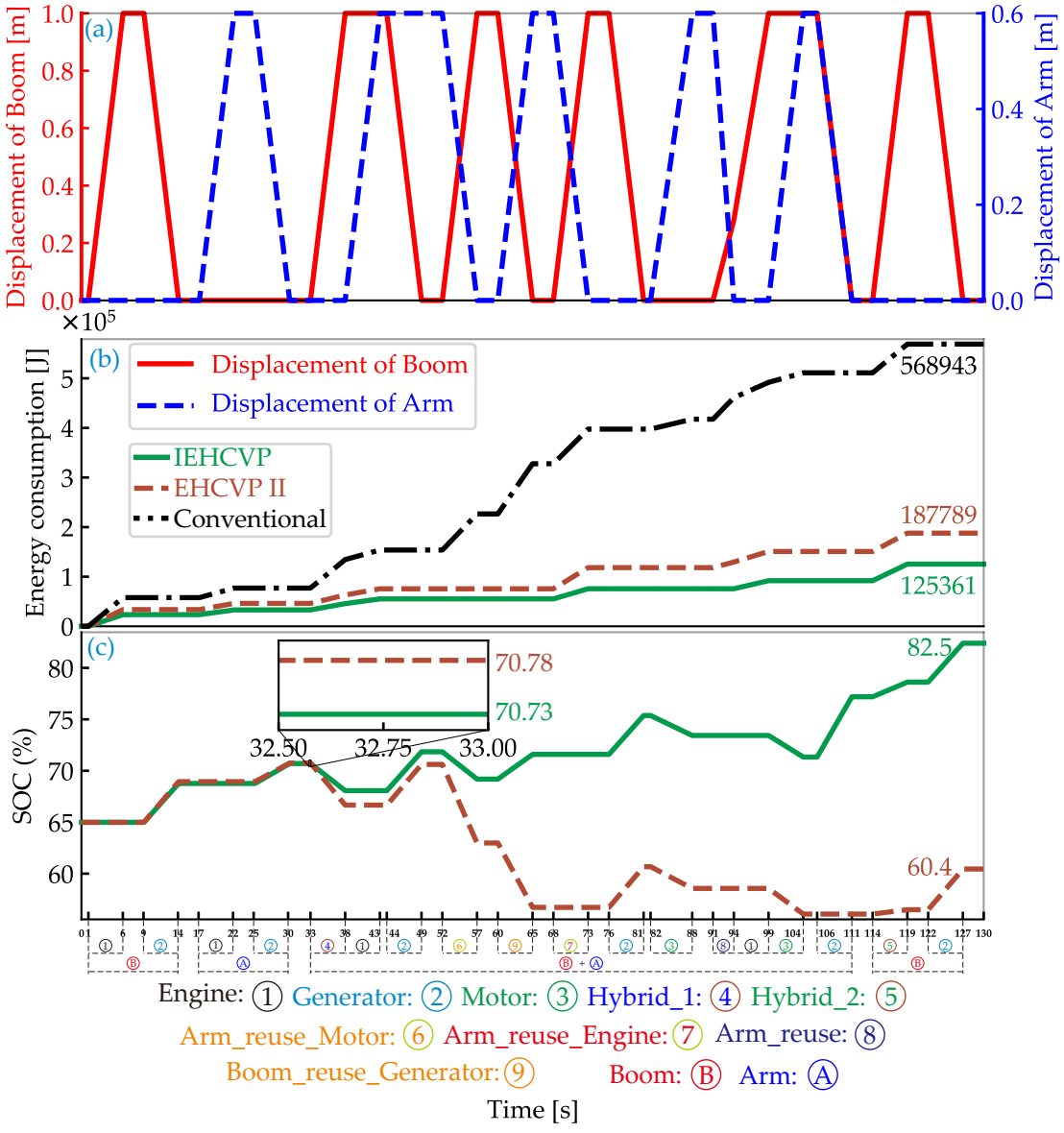

Figure 7. Displacement, energy consumption, and SOC of battery for proposed system with IEHCVP, EHCVP II, and Conventional.

The energy consumption of the ICE for each system is depicted in Figure 7b from Equations (1)–(3), (6)–(8), (14), and (16). From 1 to 43 s, the IEHCVP exhibits a lower energy output from the ICE than the EHCVP II, thanks to the integration of the CVT and ECMS. This integration leads to superior engine efficiency in the IEHCVP system. Notably, during hybrid mode #1 between 33 and 38 s, the IEHCVP effectively reduces engine energy consumption while maintaining a higher SOC than the EHCVP II. Between 60 and 65 s, the IEHCVP efficiently utilizes the energy from the boom during the arm-lowering process to drive the arm and simultaneously charge the battery. In contrast, the EHCVP II system not only fails to harness this energy but also requires power from the battery to perform this process for the motor. From 68 to 73 s, the ICE's energy supply is lower compared to the first cycle, as it benefits from the assistance provided by the energy harvested from the arm-lowering process. In comparison, the energy supplied by the engine in the EHCVP II system is more than twice as high during the same time frame. Between 91 and 94 s, both the conventional system and the EHCVP II rely on energy from the engine, while the IEHCVP system completely eliminates the need for it by harnessing energy from the arm-lowering process. This leads to a significantly reduced energy consumption in the IEHCVP system, which is remarkably efficient. During hybrid mode #2, from 114 to 119 s, the IEHCVP efficiently reduces the ICE's energy consumption while charging the battery more effectively compared to the EHCVP II system. Finally, the energy consumption of the ICE is measured as 133.976 kJ, 187.789 kJ, and 568.943 kJ for the IEHCVP, EHCVP II, and conventional systems, respectively.

The comparison of the SOC for the battery is illustrated in Figure 7c from Equations (1)–(3), (12), (13), and (17). From 1 to 33 s, the SOC of the EHCVP II was higher than that of the IEHCVP due to the use of a CVT in the IEHCVP, which is influenced by the CVT's efficiency. However, the difference is not considered significant. During hybrid mode #1, from 33 to 38 s, the IEHCVP utilizes less power from the motor, while the energy consumption from the ICE is lower compared to the EHCVP II. Between 52 and 57 s, the SOC of the EHCVP II experiences a significant decrease compared to the IEHCVP. This decrease is attributed to the EHCVP II's inability to utilize the regeneration system of the arm when it operates concurrently with the boom. Similarly, during the period from 60 to 65 s, the SOC of the EHCVP II decreases while the SOC of the IEHCVP increases. This discrepancy arises from the EHCVP II relying on the motor to supply energy to the system, whereas the IEHCVP benefits from the simultaneous regeneration of the boom. Additionally, from 106 to 111 s, the SOC of the IEHCVP increases due to the utilization of the regeneration from both the boom and the arm, while the EHCVP II does not possess this capability. Lastly, during hybrid mode #2, from 114 to 119 s, the SOC of the IEHCVP is higher than that of the EHCVP II.

Figure 8 illustrates the speed and torque of the ICE for the IEHCVP, EHCVP II, and conventional systems. By utilizing the efficiency map of the ICE shown in Figure 9a, the efficiency of each working point can be determined based on the tested speed and torque. Similarly, the working points and efficiency of the EMG can be obtained using the efficiency map in Figure 9b. Based on this information, the energy consumption of both the ICE and the EMG can be calculated. Finally, the charge and discharge energies of the battery are evaluated through the simulation process. The ICE and EMG operating points are strategically positioned within the range of the highest efficiency. To achieve this, the ratio of CVT is adjusted to match the change in each cycle as shown in Figure 10. Furthermore, the efficiency map of the CVT also achieves high efficiency, as shown in Figure 11 [47]. This is achieved by utilizing the CVT in the proposed IEHCVP system and employing the ECMS. Another factor involves the incorporation of the primary energy sources, namely the ICE and the motor, along with the supplementary energy obtained from the retraction process of the boom or arm.

To evaluate the overall energy consumption of the system, the paper proposes a calculation formula that takes into account the energy from the battery and the energy

regeneration during the retraction of the arm, which is calculated by Equation (20).

$$E_{\text{total}} = \begin{cases} E_e - \Delta E_b - \Delta E_{ra}, & \text{retraction arm} + (\text{engine or motor}) \\ E_e - \Delta E_{ra}, & \text{retraction arm} + \text{pump} \\ E_e - \Delta E_{rb}, & \text{retraction boom} + (\text{pump, generator}) \\ E_e - \Delta E_b, & \text{else} \end{cases} \tag{20}$$

where E_e represents the energy consumed by the ICE. ΔE_b denotes the change in battery charge from the beginning to the end of a process; ΔE_{bcc}, as depicted in Figure 12, denotes the change in battery charge from the beginning to the end of the current cycle, where a positive value indicates an increase in the energy stored in the battery, and vice versa. ΔE_{ra} and ΔE_{rb} refer to the energy regenerated during the retraction of the arm and boom, respectively, throughout the process. E_{total} estimates the total energy consumption of the system, which is calculated by Equation (20).

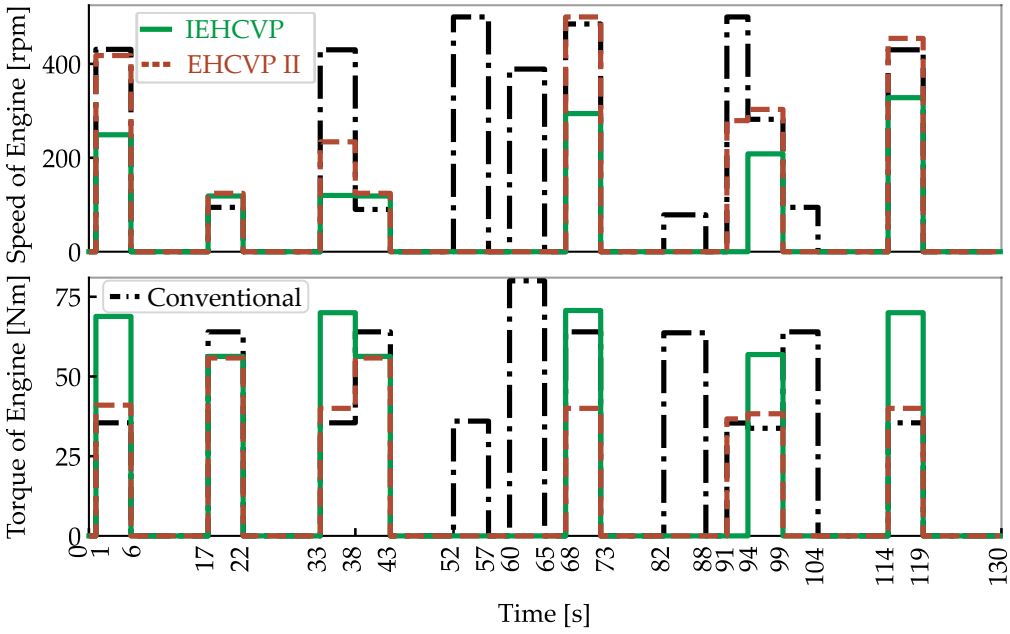

Figure 8. Speed and torque of engine for IEHCVP, EHCVP II, and Conventional.

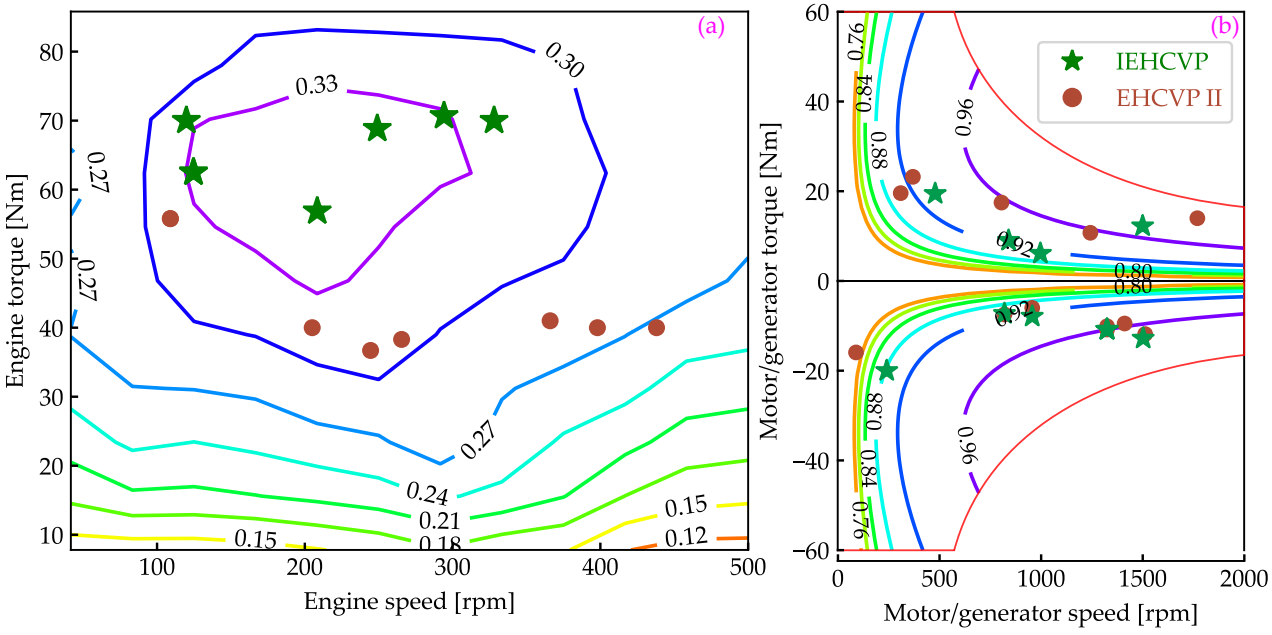

Figure 9. Working points of engine and motor/generator of proposed IEHCVP and EHCVP II.

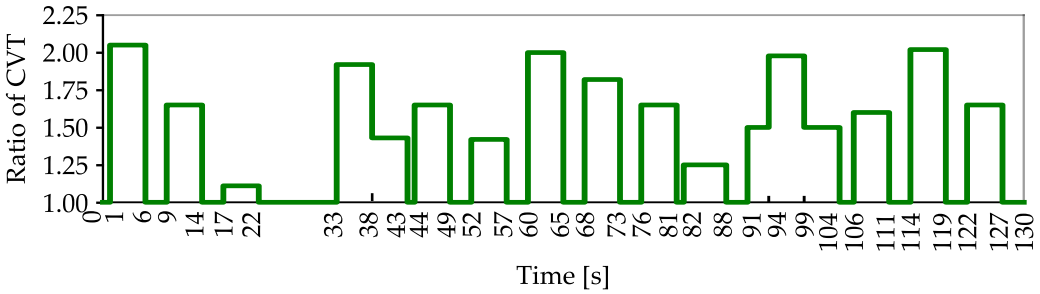

Figure 10. Ratio of CVT for IEHCVP.

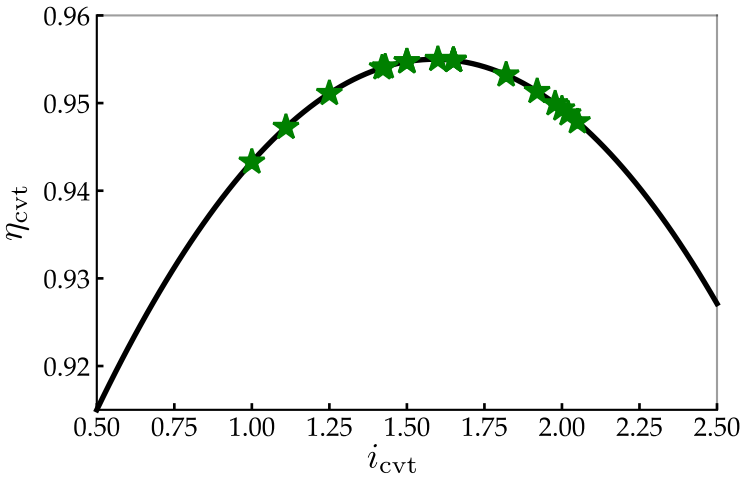

Figure 11. CVT operating efficiency.

The energy-saving efficiency is calculated by Equation (21)

$$\eta_{\mathrm{sav}} = \frac{E_{\mathrm{c}} - E_{\mathrm{total}}}{E_{\mathrm{c}}} \tag{21}$$

where η_{sav} is the energy-saving efficiency, and E_{c} is the energy consumption of the conventional system. The efficiency of the engine is a critical factor in determining the system's energy consumption. However, the energy consumption is also influenced by other components, such as the battery, boom, and arm. Consequently, a simulation was conducted to assess the overall energy consumption of the entire system. The findings, presented in Tables 4 and 5, aim to verify the energy-saving effectiveness of the proposed IEHCVP in a HE's boom and arm system.

The results are summarized in Figure 12a. The graph illustrates that the energy-saving efficiency of the IEHCVP is significantly higher than that of the EHCVP II in all cycles. For example, in stages where energy is utilized from lowering the boom and the arm, which the EHCVP II does not possess, the IEHCVP demonstrates a much superior performance. Specifically, the IEHCVP achieves an energy-saving efficiency of 79.1% within the time range from 52 to 57 s, surpassing the current EHCVP II, which achieves 63%. Moreover, the IEHCVP shows a remarkable improvement of 16.1% in the energy-saving efficiency compared to that of the EHCVP II. This improvement is attributed to the reduced energy supply from the battery due to the assistance provided by the arm-lowering process, as calculated using Equation (21). As a result, the proposed IEHCVP outperforms both the conventional system and the EHCVP II, effectively enhancing energy conservation. From 60 to 65 s, the IEHCVP demonstrates an impressive energy-saving efficiency, reaching a maximum of 85.3%. This notable accomplishment is attributed to its ability to effectively utilize the energy generated during the boom-lowering process for both battery charging and pump operation simultaneously. Such a capability sets the IEHCVP apart from conventional systems and the current EHCVP II, as they cannot achieve this level of efficiency. Here, we

can see the relationship between the hydraulic motor, pump, and generator, as shown in Equation (22). From 68 to 73 s, the EHCVP II provides more energy to the system from the engine compared to the IEHCVP, resulting in a lower energy-saving efficiency for the EHCVP II. From 91 to 94 s, the boom is fully lifted using only the energy obtained from the arm-lowering process, leading to an impressive energy-saving efficiency of 86.5% for the IEHCVP. Furthermore, it is evident that the average energy-saving efficiency throughout the entire simulation process of the IEHCVP is significantly higher than that of the current EHCVP II, specifically 77.1% compared to 60.2%, respectively.

$$T_{\mathrm{Hm}} = \frac{p_{\mathrm{c}} D_{\mathrm{Hm}} \eta_{\mathrm{Hm}}}{2\pi} = T_{\mathrm{Hpu}} + T_{\mathrm{G}} \tag{22}$$

where T_{Hm} represents the torque of the HMo, p_{c} represents the pressure of the output side of the HMo, D_{Hm} denotes the displacement of the HMo, and η_{Hm} denotes the hydro-mechanical efficiency of the HMo. T_{Hpu} and T_{G} represent the torque of the HPu and generator, respectively.

Table 4. Comparison of energy consumption between 52 and 57 s.

System	E_{e}	ΔE_{bcc}	ΔE_{b}	ΔE_{ra}	E_{total}	η_{sav}
IEHCVP	55.2	−4.95	+4.93	+3.00	47.27	0.791
EHCVP II	75.56	−15.6	−8.3	0.00	83.86	0.630
Conventional	226.53	0.00	0.00	0.00	226.53	0.00

Table 5. Comparison of energy consumption between 114 and 119 s.

System	E_{e}	ΔE_{bcc}	ΔE_{b}	ΔE_{ra}	E_{total}	η_{sav}
IEHCVP	125.36	+2.37	+19.55	0.00	105.81	0.814
EHCVP II	187.79	+0.69	−21.42	0.00	209.2	0.632
Conventional	568.94	0.00	0.00	0.00	568.94	0.00

This paper also compares the energy-saving ratios between high and medium velocities of the boom cylinder in the IEHCVP system. The results show that in the large velocity mode, the energy-saving efficiency is higher compared to the middle velocity, as shown in Figure 12b. The saving ratios for the first and third cycles are 1.16 and 1.22, respectively, as described in Table 6. The results similarly indicate that the efficiency of the EHCVP II energy-saving system is significantly higher at high speeds than at medium speeds; specifically, the saving ratios are 1.51 and 1.54 for the first and third cycles, respectively. These findings prove that the IEHCVP system performed well at both high and middle speeds. However, a significant difference exists between the two modes in the current EHCVP II system.

Table 6. Comparison between the saving ratios of high and medium velocities of boom cylinder.

Cycle		Velocities		Ratio Saving
		0.2 m/s (high)	0.1 m/s (medium)	
		η_{sav}		
1st	IEHCVP	0.594 (1–6 s)	0.509 (1–11 s)	1.16
	EHCVP II	0.418 (1–6 s)	0.277 (1–11 s)	1.51
3rd	IEHCVP	0.687 (33–38 s)	0.561 (33–43 s)	1.22
	EHCVP II	0.537 (33–38 s)	0.348 (33–43 s)	1.54

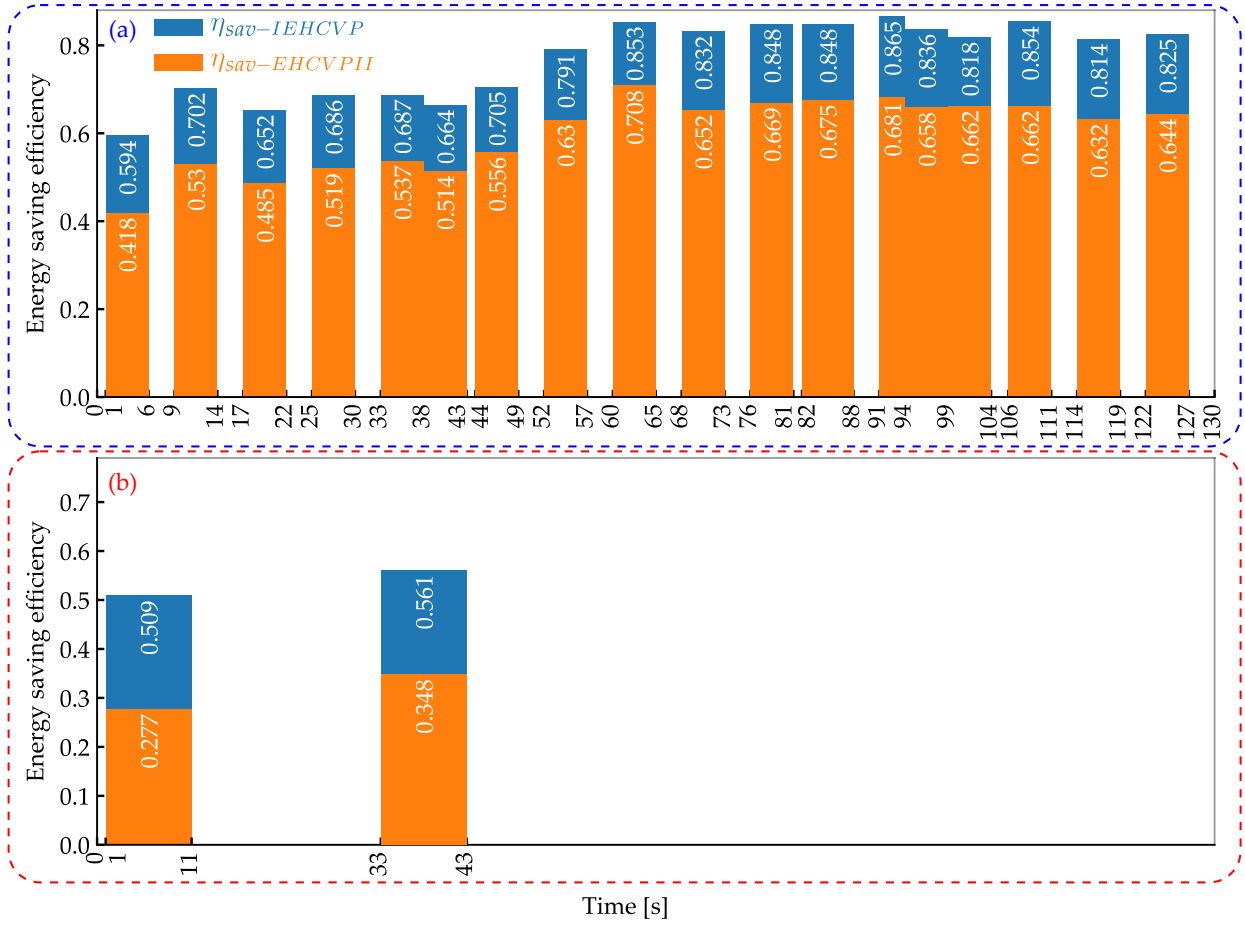

Figure 12. Energy-saving efficiency for the proposed system with IEHCVP and EHCVP II.

5. Conclusions

This paper tackled the paramount issue of energy consumption and emissions in HEs by presenting a pioneering HHE that incorporates the innovative IEHCVP and an energy regeneration system. An ECMS was also proposed as an energy management strategy, which allows the ICE's speed and torque to function within an optimal efficiency range.

The simulation results corroborated the energy-saving potential of the proposed system, indicating a decrease in energy utilization during the 'boom-up' mode. This was achieved by regenerating the boom's potential energy during the 'boom-down' mode and reutilizing it in the 'arm-up' mode. Furthermore, the combined potential energy of the arm and energy from the ICE or motor significantly contributed to the reduction in energy usage during the 'boom-up' mode.

A comparative analysis with the existing EHCVP II system and a traditional system without an EHCVP demonstrated the superior energy-saving efficiencies of the IEHCVP. Specifically, at high velocities, the proposed system was found to yield efficiencies of 16.9% and 77.1%, respectively. Similarly, at medium velocities, the system achieved energy savings of 22.25% and 53.5%, respectively. The results suggest that the proposed IEHCVP and improved ECMS can significantly enhance ICE efficiency compared to the conventional system and the current EHCVP II, proving effective in reducing energy consumption across both high and medium velocities and, thus, addressing the limitations of the current EHCVP II system.

Despite the promising results, this study also acknowledges its limitations. One prominent area was that the energy-saving efficiency in hybrid mode #1 was found to be lower than expected when compared to pure ICE mode at medium velocities. As a result, future endeavors will be focused on improving the energy-saving efficiency in all operation modes and under various conditions.

To sum up, the IEHCVP stands as a promising strategy for significantly reducing the energy consumption of HHEs. It represents a significant stride forward in the quest for more energy-efficient excavator operations, offering potential improvements to the existing systems and paving the way for future research in this area.

Author Contributions: V.H.N. carried out the investigation and methodology, built and validated the model and the proposed algorithm through AMESim simulation and Python, set up the simulation, and wrote the original manuscript. T.C.D. supported the simulation setup and checked the manuscript. K.K.A. was the supervisor providing funding and administrating the project, as well as reviewing and editing the manuscript. All authors have read and agreed to the published version of the manuscript.

Funding: This work was supported by "Regional Innovation Strategy (RIS)" through the National Research Foundation of Korea (NRF) funded by the Ministry of Education (MOE)(2021RIS-003).

Institutional Review Board Statement: Not applicable.

Informed Consent Statement: Not applicable.

Data Availability Statement: Not applicable.

Conflicts of Interest: The authors declare no conflict of interest.

Abbreviations

HEs	Hydraulic excavators
HHEs	Hybrid hydraulic excavators
EERS	Electric energy regeneration systems
HERS	Hydraulic energy regeneration systems
ICE	Internal combustion engine
EMG	Electric motor/generator
CVT	Continuously variable transmission
HPu	Hydraulic pump
HMo	Hydraulic motor
EHCVP	Electrical hydraulic continually variable powertrain
IEHCVP	Improve energy consumption of EHCVP
EMS	Energy management strategy
ECMS	Equivalent consumption minimization strategy
A-ECMS	Adaptive equivalent consumption minimization strategy
ES	Extremum seeking
EF	Equivalent factor
SOC	State of charge
BC	Boom Cylinder
AC	Arm Cylinder
VBC	Control valve of BoC
VAC	Control valve of ArC
VGB	Regeneration valve of BoC
VGA	Regeneration valve of ArC
CV	Check valve
BE	Brake of ICE
BM	Brake of EMG
BR	Brake of ring gear
BP	Brake of HPu
BH	Brake of HMo
Rin	Ring gear
Car	Carrier
Sun	Sun gear
GB	Gearbox
RL	Rotary link
ST	Sensor torque
SS	Sensor speed

SD	Sensor displacement
SV	Sensor velocity

References

1. Ding, R.; Zhang, J.; Xu, B.; Cheng, M.; Pan, M. Energy efficiency improvement of heavy-load mobile hydraulic manipulator with electronically tunable operating modes. *Energy Convers. Manag.* **2019**, *188*, 447–461. [CrossRef]
2. Zhang, S.; Minav, T.; Pietola, M.; Kauranne, H.; Kajaste, J. The effects of control methods on energy efficiency and position tracking of an electro-hydraulic excavator equipped with zonal hydraulics. *Autom. Constr.* **2019**, *100*, 129–144. [CrossRef]
3. Ge, L.; Quan, L.; Zhang, X.; Zhao, B.; Yang, J. Efficiency improvement and evaluation of electric hydraulic excavator with speed and displacement variable pump. *Energy Convers. Manag.* **2017**, *150*, 62–71. [CrossRef]
4. Chen, M.; Zhao, D. The gravitational potential energy regeneration system with closed-circuit of boom of hydraulic excavator. *Mech. Syst. Signal Process.* **2017**, *82*, 178–192. [CrossRef]
5. Wang, Z.; Jiao, X.; Pu, Z.; Han, L. Energy Recovery and Reuse Management for Fuel-electric-hydraulic Hybrid Powertrain of a Construction Vehicle. *IFAC-PapersOnLine* **2018**, *51*, 390–393. [CrossRef]
6. Li, J.; Han, Y.; Li, S. Flywheel-Based Boom Energy Recovery System for Hydraulic Excavators with Load Sensing System. *Actuators* **2021**, *10*, 126. [CrossRef]
7. Zhang, W.; Wang, J.; Du, S.; Ma, H.; Zhao, W.; Li, H. Energy Management Strategies for Hybrid Construction Machinery: Evolution, Classification, Comparison and Future Trends. *Energies* **2019**, *12*, 2024. [CrossRef]
8. Ge, L.; Dong, Z.; Quan, L.; Li, Y. Potential energy regeneration method and its engineering applications in large-scale excavators. *Energy Convers. Manag.* **2019**, *195*, 1309–1318. [CrossRef]
9. Shen, W.; Jiang, J.; Su, X.; Reza Karimi, H. Control strategy analysis of the hydraulic hybrid excavator. *J. Frankl. Inst.* **2015**, *352*, 541–561. [CrossRef]
10. Mu, H.; Luo, Y.; Luo, Y.; Chen, L. Numerical Analysis of Energy Recovery of Hybrid Loader Actuators Based on Parameters Optimization. *Actuators* **2022**, *11*, 260. [CrossRef]
11. Yu, Y.X.; Ahn, K.K. Optimization of energy regeneration of hybrid hydraulic excavator boom system. *Energy Convers. Manag.* **2019**, *183*, 26–34. [CrossRef]
12. Wang, T.; Wang, Q. Efficiency analysis and evaluation of energy-saving pressure-compensated circuit for hybrid hydraulic excavator. *Autom. Constr.* **2014**, *47*, 62–68. [CrossRef]
13. Minav, T.; Virtanen, A.; Laurila, L.; Pyrhönen, J. Storage of energy recovered from an industrial forklift. *Autom. Constr.* **2012**, *22*, 506–515. [CrossRef]
14. Yu, Y.; Do, T.C.; Park, Y.; Ahn, K.K. Energy saving of hybrid hydraulic excavator with innovative powertrain. *Energy Convers. Manag.* **2021**, *244*, 114447. [CrossRef]
15. Ge, L.; Quan, L.; Li, Y.; Zhang, X.; Yang, J. A novel hydraulic excavator boom driving system with high efficiency and potential energy regeneration capability. *Energy Convers. Manag.* **2018**, *166*, 308–317. [CrossRef]
16. Lin, T.; Wang, Q.; Hu, B.; Gong, W. Development of hybrid powered hydraulic construction machinery. *Autom. Constr.* **2010**, *19*, 11–19. [CrossRef]
17. Do, T.C.; Nguyen, D.G.; Dang, T.D.; Ahn, K.K. A Boom Energy Regeneration System of Hybrid Hydraulic Excavator Using Energy Conversion Components. *Actuators* **2021**, *10*, 1. [CrossRef]
18. Yu, Y.; Ahn, K.K. Energy Regeneration and Reuse of Excavator Swing System with Hydraulic Accumulator. *Int. J. Precis. Eng. -Manuf.-Green Technol.* **2019**, *7*, 859–873. [CrossRef]
19. Ahn, K.K.; Hung, T.; Dinh, T. A Study on Energy Saving Potential of Hydraulic Control System Using Switching Type Closed Loop Constant Pressure System. *Proc. JFPS Int. Symp. Fluid Power* **2008**, *2008*. [CrossRef]
20. Xia, L.; Quan, L.; Ge, L.; Hao, Y. Energy efficiency analysis of integrated drive and energy recuperation system for hydraulic excavator boom. *Energy Convers. Manag.* **2018**, *156*, 680–687. [CrossRef]
21. Ho, T.H.; Le, T.D. Development and Evaluation of Energy-Saving Electro-Hydraulic Actuator. *Actuators* **2021**, *10*, 302. [CrossRef]
22. Do, T.C.; Dang, T.D.; Dinh, T.Q.; Ahn, K.K. Developments in energy regeneration technologies for hydraulic excavators: A review. *Renew. Sustain. Energy Rev.* **2021**, *145*, 111076. [CrossRef]
23. Yu, Y.; Do, T.C.; Yin, B.; Ahn, K.K. Improvement of Energy Saving for Hybrid Hydraulic Excavator with Novel Powertrain. *Int. J. Precis. Eng. -Manuf.-Green Technol.* **2022**, *10*, 521–534. [CrossRef]
24. Zhou, D.; Ravey, A.; Al-Durra, A.; Gao, F. A comparative study of extremum seeking methods applied to online energy management strategy of fuel cell hybrid electric vehicles. *Energy Convers. Manag.* **2017**, *151*, 778–790. [CrossRef]
25. Paganelli, G.; Delprat, S.; Guerra, T.; Rimaux, J.; Santin, J. Equivalent consumption minimization strategy for parallel hybrid powertrains. In Proceedings of the Vehicular Technology Conference. IEEE 55th Vehicular Technology Conference. VTC Spring 2002 (Cat. No.02CH37367), Birmingham, AL, USA, 6–9 May 2002; Volume 4, pp. 2076–2081. [CrossRef]
26. Adaptive Equivalent Consumption Minimization Strategy for Hybrid Electric Vehicles. In Proceedings of the ASME 2010 Dynamic Systems and Control Conference, Volume 1, Dynamic Systems and Control Conference, Cambridge, MA, USA, 12–15 September 2010. [CrossRef]
27. Sun, C.; Sun, F.; He, H. Investigating adaptive-ECMS with velocity forecast ability for hybrid electric vehicles. *Appl. Energy* **2017**, *185*, 1644–1653. [CrossRef]

28. Tian, X.; Cai, Y.; Sun, X.; Zhu, Z.; Xu, Y. An adaptive ECMS with driving style recognition for energy optimization of parallel hybrid electric buses. *Energy* **2019**, *189*, 116151. [CrossRef]
29. EL-Seesy, A.I.; He, Z.; Hassan, H.; Balasubramanian, D. Improvement of combustion and emission characteristics of a diesel engine working with diesel/jojoba oil blends and butanol additive. *Fuel* **2020**, *279*, 118433. [CrossRef]
30. Zhang, F.; Appiah, D.; Hong, F.; Zhang, J.; Yuan, S.; Adu-Poku, K.A.; Wei, X. Energy loss evaluation in a side channel pump under different wrapping angles using entropy production method. *Int. Commun. Heat Mass Transf.* **2020**, *113*, 104526. [CrossRef]
31. Fresia, P.; Rundo, M.; Padovani, D.; Altare, G. Combined speed control and centralized power supply for hybrid energy-efficient mobile hydraulics. *Autom. Constr.* **2022**, *140*, 104337. [CrossRef]
32. Wang, Y.; Li, K.; Zeng, X.; Gao, B.; Hong, J. Energy consumption characteristics based driving conditions construction and prediction for hybrid electric buses energy management. *Energy* **2022**, *245*, 123189. [CrossRef]
33. Jun, G.; Daqing, Z.; Yong, G.; Zhongyong, T.; Changsheng, L.; Peng, H.; Yuming, Z.; Weicai, Q.; Yongping, J. Potential energy recovery method based on alternate recovery and utilization of multiple hydraulic cylinders. *Autom. Constr.* **2020**, *112*, 103105. [CrossRef]
34. Schmid, R.; Bürger, J.; Bajcinca, N. A comparison of PMP-based Energy Management Strategies for Plug-in-Hybrid Electric Vehicles. *IFAC-PapersOnLine* **2019**, *52*, 592–597. [CrossRef]
35. Teodorescu, C.S.; Vandenplas, S.; Depraetere, B.; Shariatmadar, K.; Vyncke, T.; Duflou, J.; Nowé, A. An ECMS-based powertrain control of a parallel hybrid electric forklift. In Proceedings of the 2017 21st International Conference on System Theory, Control and Computing (ICSTCC), Sinaia, Romania, 19–21 October 2017; pp. 763–770. [CrossRef]
36. Wang, Y.; Sun, Z. SDP-based extremum seeking energy management strategy for a power-split hybrid electric vehicle. In Proceedings of the 2012 American Control Conference (ACC), Montreal, QC, Canada, 27–29 June 2012; pp. 553–558. [CrossRef]
37. Fröberg, A.; Åslund, J.; Nielsen, L. Optimal transient control of power generation in hybrid construction equipment. In Proceedings of the 2011 IEEE Vehicle Power and Propulsion Conference, Chicago, IL, USA, 6–9 September 2011; pp. 1–6. [CrossRef]
38. Zeng, X.; Yang, N.; Song, D.; Zhang, C.; Wang, J.; Wang, J.; Wang, Q. Multi-factor integrated parametric design of power-split hybrid electric bus. *J. Clean. Prod.* **2016**, *115*, 88–100. [CrossRef]
39. Wei, C.; Chen, Y.; Sun, X.; Zhang, Y. Optimal Equivalent Consumption Minimization Strategy for Plug-In Hybrid Electric Vehicle with Improved Genetic Algorithm. *SAE Int. J. Electrified Veh.* **2020**, *9*, 143–154. [CrossRef]
40. Liu, X.; Qin, D.; Wang, S. Minimum Energy Management Strategy of Equivalent Fuel Consumption of Hybrid Electric Vehicle Based on Improved Global Optimization Equivalent Factor. *Energies* **2019**, *12*, 2076. [CrossRef]
41. Zhou, D.; Al-Durra, A.; Matraji, I.; Ravey, A.; Gao, F. Online Energy Management Strategy of Fuel Cell Hybrid Electric Vehicles: A Fractional-Order Extremum Seeking Method. *IEEE Trans. Ind. Electron.* **2018**, *65*, 6787–6799. [CrossRef]
42. Cai, Y.; Ouyang, M.; Yang, F. Impact of power split configurations on fuel consumption and battery degradation in plug-in hybrid electric city buses. *Appl. Energy* **2017**, *188*, 257–269. [CrossRef]
43. Komatsu Corporation. Komatsu 107E-1 Series Diesel Engine Shop Manual. 2013. Available online: https://issuu.com/heydownloads/docs/komatsu__107e-1_series_diesel_engine_shop_manual__ (accessed on 1 September 2023).
44. X-Engineer. Brake Specific Fuel Consumption of the Internal Combustion Engines. 2017. Available online: https://x-engineer.org/brake-specific-fuel-consumption-bsfc/ (accessed on 1 September 2023).
45. Hyundai Corporation. AC Induction Motor Data Sheet. 2011. Available online: http://www.hyundaimotorkorea.com/wp-content/uploads/2015/11/%ED%98%84%EB%8C%80%EA%B3%A0%ED%9A%A8%EC%9C%A8%EB%AA%A8%ED%84%B0-5.5KW-2P-B3-AL-%EC%82%AC%EC%96%91%EC%84%9C.pdf (accessed on 1 September 2023).
46. Hu, B.; Li, J. A Deployment-Efficient Energy Management Strategy for Connected Hybrid Electric Vehicle Based on Offline Reinforcement Learning. *IEEE Trans. Ind. Electron.* **2022**, *69*, 9644–9654. [CrossRef]
47. Ruan, J. Comparing of Single Reduction and CVT Based Transmissions on Battery. Electric Vehicle. 10. 2015. Available online: https://doi.org/10.6567/IFToMM.14TH.WC.OS17.010 (accessed on 1 September 2023).